PERGAMON

International Journal of Solids and Structures 39 (2002) 1621–1650

INTERNATIONAL JOURNAL OF SOLIDS and STRUCTURES

www.elsevier.com/locate/ijsolstr

Numerical and analytical solutions for the problem of hydraulic fracturing from a cased and cemented wellbore

C. Atkinson [a,*], D.A. Eftaxiopoulos [b]

[a] *Department of Mathematics, Imperial College of Science, Technology and Medicine, Huxley Building, 180 Queen's Gate, London SW7 2BZ, UK*

[b] *Department of Mechanics, Faculty of Applied Sciences, National Technical University of Athens, Zografou Campus, GR-15773, Athens, Greece*

Received 28 June 2000

Abstract

Numerical and analytical investigations of the hydraulic fracture propagation problem, from a cased and cemented wellbore, have been pursued in this communication. A two-dimensional plane model has been used. Pure bond and pure slip boundary conditions, along the steel/cement and the cement/rock interfaces have been implemented, as two extreme cases. Both the in-plane and the anti-plane problems have been considered. Analytical and numerical methods have been applied to the problem of a straight fracture, while in the curved crack case only a numerical solution has been adopted. Crack turning is found to depend on the elastic properties of the rock in the pure bond case, while in the pure slip case no turning occurs. Results indicate that in the pure slip case, a larger pressure than that of the pure bond case, is required at the first propagation step. Results related to a starter (i.e. at the first propagation step) crack lying parallel to the plane of the maximum remote principal stress while the elastic modulus of the rock varies, indicate that bigger values, for both the pressure and the mode I crack opening displacement (COD) at the open hole, develop in the pure slip case than in the pure bond case. Results concerning a starter crack, inclined at varying angles with respect to the plane of the maximum remote principal stress, show that the mode II COD at the open hole is bigger in the pure bond case than in the pure slip case, for all the angles of inclination.

Keywords: Hydraulic fracturing; Two-dimensional model; Casing; Cement; Rock; Pure bond; Pure slip

1. Introduction

Deviated wells are increasingly used in oil recovery. Multi-directional drilling can thus be pursued from a single platform and also particular reservoirs and rocks, whose geometry and properties are highly orientation dependent, can be treated more efficiently. Hydraulic fracturing is however often problematic when initiated from an inclined wellbore. In that case the state of stresses near the well changes and the prediction of the fracture surface is not immediately attainable. The turning and twisting of the crack is

* Corresponding author. Tel.: +44-20-7589-5111; fax: +44-20-7589-8517.
E-mail address: c.atkinson@ic.ac.uk (C. Atkinson).

0020-7683/02/$ - see front matter
PII: S0020-7683(01)00259-1

often coupled with the generation of multiple fractures. The fracturing fluid advance can thus be severely impeded and this may lead to an early screen out, i.e. inadvertent plugging of the well with the granular substance carried by the fracturing fluid.

The fracturing process becomes more complicated when the wellbore is cased and cemented, since this imposes a new stress situation around the well. It has been observed that the crack may initially extend along the cement/rock interface before entering the rock itself. New stress concentrations are also induced at the tips of perforations which may change the preferable plane for fracture initiation.

Yew and Li (1987) and Yew et al. (1989) have applied 3D elasticity theory in order to study hydraulically induced fractures from inclined wellbores. The growth and link up of mini cracks initiated at the perforations of a cased wellbore, are investigated by Yew et al. (1993). A 3D analysis of the fracturing process from an inclined well, via the use of a numerical simulator, has been presented by Morales and Brady (1993). The initiation, interaction and propagation of fractures from a deviated well have been studied by Weng (1993). The effect of casing on the hydraulic fracture have been considered by Carter et al. (1994). Romero et al. (1995) have investigated several near wellbore effects like fracture reorientation, perforation phasing misalignment, perforation pressure drop etc. Atkinson and Thiercelin (1993) have studied the interaction between an open hole and pressure induced fractures of mode I. Eftaxiopoulos and Atkinson (1996) studied numerically a plane model of hydraulic fracture propagation from a cased, cemented and inclined wellbore, considering perfect bond between the steel/cement and the cement–rock interfaces.

In this study, the crack propagation from a cased, cemented and inclined wellbore is considered by using two-dimensional (2D) in-plane and anti-plane elasticity analysis. Thus, all the three modes of crack opening displacements (CODs), i.e. tensile, in-plane shear and out-of-plane shear, are incorporated. The pressure is kept constant along the crack. The path of the crack is determined by the maximum normal stress criterion, applied ahead of the crack tip. Two extreme cases of boundary conditions along the steel/cement and the cement/rock interfaces are considered. Perfect bond where continuity of stresses and displacements is implied and perfect slip where zero shear stress and continuity of normal stresses and displacements are considered. For the sake of simplicity, we consider that the crack lies in an infinite medium, loaded by the stresses calculated by Atkinson and Eftaxiopoulos (1996) for the perfect bond case or the field calculated in Sections 2.2.1 and 2.2.2 of this work, for the perfect slip case. When the crack is curved (in the perfect bond case for rocks with low elasticity modulus), a numerical method is used for the solution of a system of integral equations at each propagation step. When the fracture is straight, both a numerical and an analytical solution are possible and a comparison of the corresponding results is made.

The optimum initial crack orientation is determined by the stress field along the cement/rock interface, which in turn depends on the elastic properties of the rock, as far as the perfect bond case is concerned (Atkinson and Eftaxiopoulos, 1996). In fact, the starter fracture is found to lie either at 90° or at 0° with respect to plane of the maximum remote stress σ_h (see Fig. 1).

In the perfect slip case, results indicate that the plane of the maximum tangential stress along the cement/rock interface, is always parallel to the plane of the maximum remote stress σ_h and independent of the rock elastic properties. Mode I and III CODs are more severe close to the well in the straight crack case and around the middle of the crack in the curved fracture case. In the curved crack instance, the mode II COD is more intense close to the well. The presence of the casing and the cement leads to the reduction of the CODs of all modes near the wellbore, as expected. A larger pressure is required at the first propagation step in the pure slip case, than that in the pure bond case. Mode I opening and mode III sliding displacements along a straight crack at the final propagation step, remain virtually unaltered when the boundary conditions around the wellbore change from pure bond to pure slip.

Results related to a starter crack lying parallel to the plane of the maximum remote principal stress while the elastic modulus of the rock varies, indicate that bigger values, for both the pressure and the mode I COD at the open hole, develop in the pure slip case than in the pure bond case. The mode III COD at

$r = R_1$ increases with increasing $E^{(3)}$, possibly indicating a more severe tendency for twist of the fracture in stiffer rocks.

Results concerning a starter crack, inclined at varying angles with respect to the plane of the maximum remote principal stress while the elastic modulus of the rock remains constant, show that the pressure is greater for the pure slip case than for the pure bond one, for inclinations smaller than roughly 45°, while the opposite happens for inclinations bigger than roughly 45°. Also the mode I COD decreases as the starter crack rotates, approaching the plane of the minimum remote stress, while values for the pure slip case are generally bigger than those for the pure bond case. The mode II COD at the open hole is bigger in the pure bond case than in the pure slip case, for all the angles of inclination. Changing signs in the variation of the mode III COD at the open hole may point to different angles of twist of a real 3D crack.

2. The stress field around a cased and cemented wellbore

We consider a planar cross-section of the cased and cemented wellbore, in the state of plane strain, as shown in Fig. 1. The fracture is initially absent. In the far field, in-plane principal stresses σ_H and σ_h are

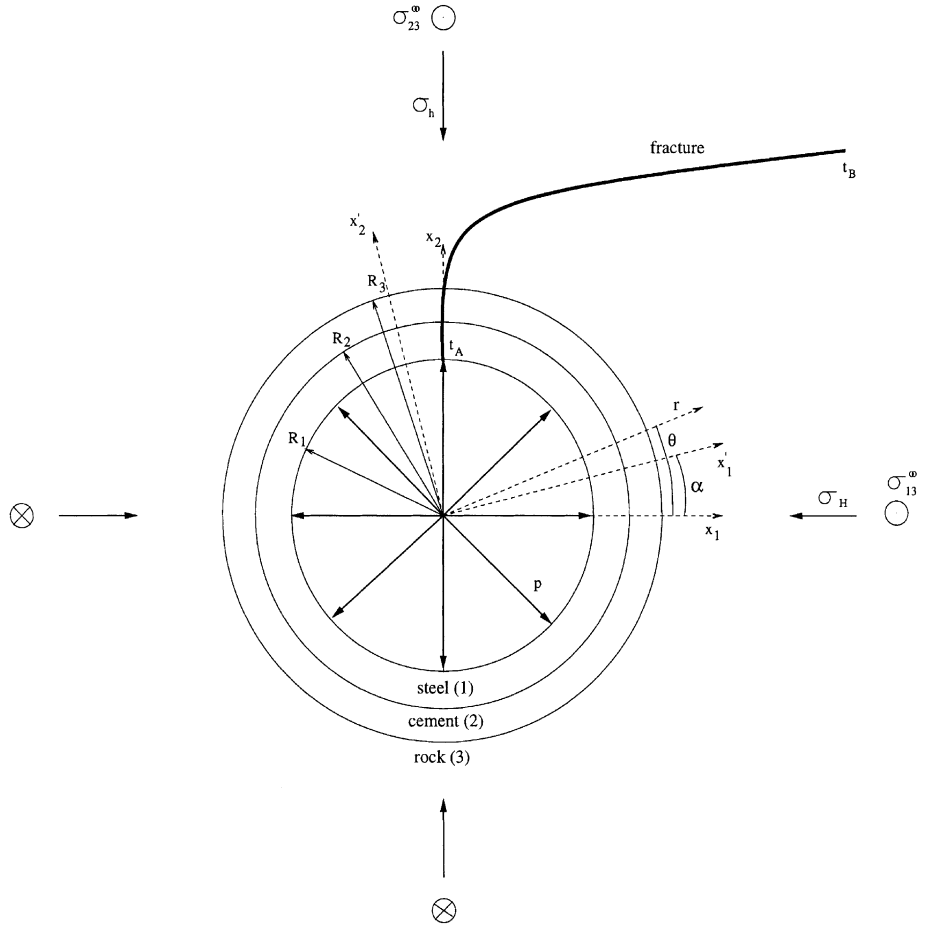

Fig. 1. A plane cross-section of a fractured inclined, cased and cemented wellbore, remotely loaded by in-plane and anti-plane stresses.

applied, with the latter having a smaller absolute value than the former. Remote anti-plane stresses σ_{13}^{∞} and σ_{23}^{∞} are also considered, for the case of an inclined wellbore to be simulated. The radii of the open hole, the steel/cement interface and the cement/rock interface are R_1, R_2 and R_3 respectively. Internal pressure p is applied on the steel annulus internally. Both a Cartesian coordinate system $O(x_1, x_2)$ and a polar coordinate system $O(r, \theta)$ (see Fig. 1) are used. Superscripts (1), (2), (3) refer to the steel, the cement and the rock respectively. μ is the shear modulus and v is the Poisson's ratio.

Two cases have been considered, for the interfaces along the steel/cement and the cement/rock annuli. The perfect bond condition where there is continuity of stresses and displacements along the interfaces and the perfect slip condition where there is continuity of normal stresses and normal displacements, but the shear stress is zero along these interfaces. Neither of these two conditions is realistic, since the situation on the interfaces may be more complicated (e.g. friction may develop). However, these two extreme boundary conditions, provide two bounds for the actual stress situation around the wellbore.

2.1. Perfect bond at the steel/cement and cement/rock interfaces

The stress field for the perfect bond case has been evaluated by Atkinson and Eftaxiopoulos (1996), for both the in-plane and the anti-plane problems. In that article, results indicated that the plane of the maximum tangential stress $\sigma_{\theta\theta}$, along the steel/cement and the cement/rock interfaces, may rotate at 90° with respect to the plane of the maximum remote stress σ_h, depending on the value of the Young's modulus of the rock. Such a rotation will force the hydraulic fracture to turn when it propagates far away from the wellbore (see Section 3.1).

2.2. Perfect slip at the steel/cement and cement/rock interfaces

In the following we develop the expressions for the stresses and displacements for the perfect slip case, for both the in-plane and the anti-plane problems.

2.2.1. In-plane problem

Since we have a state of plane strain, $u_3 = 0$ and the field is taken to be independent of x_3. Stresses and displacements are given by Coker and Filon (1957) by

$$\sigma_{rr} = \frac{1}{r^2}\frac{\partial^2\chi}{\partial\theta^2} + \frac{1}{r}\frac{\partial\chi}{\partial r} \tag{1}$$

$$\sigma_{\theta\theta} = \frac{\partial^2\chi}{\partial\theta^2} \tag{2}$$

$$\sigma_{r\theta} = -\frac{\partial}{\partial r}\left(\frac{1}{r}\frac{\partial\chi}{\partial\theta}\right) \tag{3}$$

$$2\mu u_r = -\frac{\partial\chi}{\partial r} + (1-v)r\frac{\partial\psi}{\partial\theta} \tag{4}$$

$$2\mu u_\theta = -\frac{1}{r}\frac{\partial\chi}{\partial\theta} + (1-v)r^2\frac{\partial\psi}{\partial r} \tag{5}$$

provided that

$$\nabla^2\psi = 0 \tag{6}$$

$$\frac{\partial}{\partial r}\left(r\frac{\partial \psi}{\partial \theta}\right) = \nabla^2 \chi \tag{7}$$

$$\nabla^4 \chi = 0 \tag{8}$$

$\chi(r,\theta)$ and $\psi(r,\theta)$ are real functions to be determined.

In the extreme case where the rock/cement and cement/steel interfaces are allowed to slip freely, i.e. without any friction developing between them, the boundary conditions are

$$\text{On } r \to \infty: \quad \sigma_{11}^{(3)} = \sigma_{\mathrm{H}} \tag{9}$$

$$\sigma_{22}^{(3)} = \sigma_{\mathrm{h}} \tag{10}$$

$$\text{On } r = R_3: \quad \sigma_{rr}^{(2)} = \sigma_{rr}^{(3)} \tag{11}$$

$$u_r^{(2)} = u_r^{(3)} \tag{12}$$

$$\sigma_{r\theta}^{(2)} = 0 \tag{13}$$

$$\sigma_{r\theta}^{(3)} = 0 \tag{14}$$

$$\text{On } r = R_2: \quad \sigma_{rr}^{(1)} = \sigma_{rr}^{(2)} \tag{15}$$

$$u_r^{(1)} = u_r^{(2)} \tag{16}$$

$$\sigma_{r\theta}^{(1)} = 0 \tag{17}$$

$$\sigma_{r\theta}^{(2)} = 0 \tag{18}$$

$$\text{On } r = R_1: \quad \sigma_{rr}^{(1)} = p \tag{19}$$

$$\sigma_{r\theta}^{(1)} = 0 \tag{20}$$

We can choose as functions $\chi(r,\theta)$ and $\psi(r,\theta)$ the following

$$\chi^{(3)}(r,\theta) = \frac{(\sigma_{\mathrm{H}} + \sigma_{\mathrm{h}})}{4} r^2 - \frac{(\sigma_{\mathrm{H}} - \sigma_{\mathrm{h}})}{4} r^2 \cos 2\theta + \frac{A^{(3)}}{2} \cos 2\theta + B^{(3)} r^{-2} \cos 2\theta + G^{(3)} \ln r \tag{21}$$

$$\psi^{(3)}(r,\theta) = (\sigma_{\mathrm{H}} + \sigma_{\mathrm{h}})\theta + A^{(3)} r^{-2} \sin 2\theta \tag{22}$$

$$\chi^{(2)}(r,\theta) = \frac{A^{(2)}}{2} \cos 2\theta + B^{(2)} r^{-2} \cos 2\theta + C^{(2)} r^2 \cos 2\theta + \frac{D^{(2)}}{2} r^4 \cos 2\theta + \frac{F^{(2)}}{4} r^2 + G^{(2)} \ln r \tag{23}$$

$$\psi^{(2)}(r,\theta) = A^{(2)} r^{-2} \sin 2\theta + D^{(2)} r^2 \sin 2\theta + F^{(2)}\theta \tag{24}$$

$$\chi^{(1)}(r,\theta) = \frac{A^{(1)}}{2} \cos 2\theta + B^{(1)} r^{-2} \cos 2\theta + C^{(1)} r^2 \cos 2\theta + \frac{D^{(1)}}{2} r^4 \cos 2\theta + \frac{F^{(1)}}{4} r^2 + G^{(1)} \ln r \tag{25}$$

$$\psi^{(1)}(r,\theta) = A^{(1)} r^{-2} \sin 2\theta + D^{(1)} r^2 \sin 2\theta + F^{(1)}\theta \tag{26}$$

Inserting the right-hand side of Eqs. (21)–(26) into Eqs. (1)–(5), we get the expressions for the stresses and displacements as

$$\sigma_{rr}^{(3)} = \frac{(\sigma_H + \sigma_h)}{2} + \frac{(\sigma_H - \sigma_h)}{2}\cos 2\theta - 2A^{(3)}r^{-2}\cos 2\theta - 6B^{(3)}r^{-4}\cos 2\theta + G^{(3)}r^{-2} \tag{27}$$

$$\sigma_{\theta\theta}^{(3)} = \frac{(\sigma_H + \sigma_h)}{2} - \frac{(\sigma_H - \sigma_h)}{2}\cos 2\theta + 6B^{(3)}r^{-4}\cos 2\theta - G^{(3)}r^{-2} \tag{28}$$

$$\sigma_{r\theta}^{(3)} = -\frac{(\sigma_H - \sigma_h)}{2}\sin 2\theta - A^{(3)}r^{-2}\sin 2\theta - 6B^{(3)}r^{-4}\sin 2\theta \tag{29}$$

$$2\mu^{(3)}u_r^{(3)} = -\frac{(\sigma_H + \sigma_h)}{2}r + \frac{(\sigma_H - \sigma_h)}{2}r\cos 2\theta + 2B^{(3)}r^{-3}\cos 2\theta - G^{(3)}r^{-1} + (1 - \nu^{(3)})r \times \left[\sigma_H + \sigma_h + 2A^{(3)}r^{-2}\cos 2\theta\right] \tag{30}$$

$$2\mu^{(3)}u_\theta^{(3)} = -\frac{(\sigma_H - \sigma_h)}{2}r\sin 2\theta - (1 - 2\nu^{(3)})A^{(3)}r^{-1}\sin 2\theta + 2B^{(3)}r^{-3}\sin 2\theta \tag{31}$$

$$\sigma_{rr}^{(2)} = -2A^{(2)}r^{-2}\cos 2\theta - 6B^{(2)}r^{-4}\cos 2\theta - 2C^{(2)}\cos 2\theta + \frac{F^{(2)}}{2} + G^{(2)}r^{-2} \tag{32}$$

$$\sigma_{\theta\theta}^{(2)} = 6B^{(2)}r^{-4}\cos 2\theta + 2C^{(2)}\cos 2\theta + 6D^{(2)}r^2\cos 2\theta + \frac{F^{(2)}}{2} - G^{(2)}r^{-2} \tag{33}$$

$$\sigma_{r\theta}^{(2)} = -A^{(2)}r^{-2}\sin 2\theta - 6B^{(2)}r^{-4}\sin 2\theta + 2C^{(2)}\sin 2\theta + 3D^{(2)}r^2\sin 2\theta \tag{34}$$

$$2\mu^{(2)}u_r^{(2)} = 2(1 - \nu^{(2)})A^{(2)}r^{-1}\cos 2\theta + 2B^{(2)}r^{-3}\cos 2\theta - 2C^{(2)}\cos 2\theta - 2\nu^{(2)}D^{(2)}r^3\cos 2\theta + (1/2 - \nu^{(2)})rF^{(2)} - r^{-1}G^{(2)} \tag{35}$$

$$2\mu^{(2)}u_\theta^{(2)} = -(1 - 2\nu^{(2)})A^{(2)}r^{-1}\sin 2\theta + 2B^{(2)}r^{-3}\sin 2\theta + 2C^{(2)}\sin 2\theta + (3 - 2\nu^{(2)})D^{(2)}r^3\sin 2\theta \tag{36}$$

The relations for the field in the steel can be obtained from Eqs. (32)–(36), if the superscript (2) is replaced by (1). Inserting the formuli (27), (29), (30), (32), (34) and (35), into the boundary conditions (11)–(20), we end up with a system of 15 linear equations with 15 unknown constants $A^{(3)}$, $B^{(3)}$, $G^{(3)}$, $A^{(j)}$, $B^{(j)}$, $C^{(j)}$, $D^{(j)}$, $F^{(j)}$, $G^{(j)}$, $j = 1, 2$, which is solved numerically. Note that the conditions (9) and (10) are automatically satisfied.

2.2.2. Anti-plane problem

For the anti-plane problem, the shear stresses at infinity are σ_{13}^{∞} and σ_{23}^{∞}. The stresses σ_{13}, σ_{23} and the displacement u_3 are given by Kanninen and Popelar (1985), in terms of a complex potential $f(z)$, as

$$\sigma_{13} - \mathrm{i}\sigma_{23} = 2f'(z) \tag{37}$$

$$u_3 = \frac{1}{\mu}\left[f(z) + \overline{f(z)}\right] \tag{38}$$

The transformation formula that gives the stresses σ_{r3}, $\sigma_{\theta 3}$ with reference to the polar coordinate system $\mathrm{O}(r, \theta, x_3)$ in terms of the stresses σ_{13}, σ_{23}, is

$$\sigma_{r3} - \mathrm{i}\sigma_{\theta 3} = \mathrm{e}^{\mathrm{i}\theta}[\sigma_{13} - \mathrm{i}\sigma_{23}] \tag{39}$$

The boundary conditions of the problem are now the following:

$$\text{On } r \to \infty: \quad \sigma_{13}^{(3)} - \mathrm{i}\sigma_{23}^{(3)} = \sigma_{13}^{\infty} - \mathrm{i}\sigma_{23}^{\infty} \tag{40}$$

$$\text{On } r = R_3: \quad \sigma_{r3}^{(3)} = 0 \tag{41}$$

$$\sigma_{r3}^{(2)} = 0 \tag{42}$$

$$\text{On } r = R_2: \quad \sigma_{r3}^{(2)} = 0 \tag{43}$$

$$\sigma_{r3}^{(1)} = 0 \tag{44}$$

$$\text{On } r = R_1: \quad \sigma_{r3}^{(1)} = 0 \tag{45}$$

We choose

$$f'^{(3)}(z) = A^{(3)} + \frac{B^{(3)}}{z^2} \tag{46}$$

where the prime again denotes differentiation with respect to the complex variable z. $A^{(3)}$ can be immediately determined as

$$A^{(3)} = \frac{\sigma_{13}^{\infty} - \mathrm{i}\sigma_{23}^{\infty}}{2} \tag{47}$$

from Eqs. (39) and (46). From Eqs. (41) and (47) we can extract

$$B^{(3)} = -R_3^2 \overline{A^{(3)}} \tag{48}$$

The stresses and displacements in the cement and the steel annuli are zero since no anti-plane shear stresses act on their boundaries.

3. Numerical solution for a curved crack emanating from a cased and cemented wellbore

As pointed out by Atkinson and Eftaxiopoulos (1996) and Eftaxiopoulos and Atkinson (1996), the plane of the maximum tangential stress $\sigma_{\theta\theta}$ along the cement/rock interface may be at an angle of 90° with that of the maximum remote stress σ_{h}, as long as the pure bond case for the steel/cement and the cement/rock interfaces is concerned. Thus the fracture may turn at 90° while it propagates away from the wellbore, for particular rock elastic properties and particular radii of the open hole and the steel and cement annuli.

In this section, a curved crack is considered open at the point t_{A} of the open hole, propagating in the rock and terminating at the point t_{B} (Fig. 1). The numerical procedure presented below, applies to the straight crack case as well and is similar to the one followed by Eftaxiopoulos and Atkinson (1996).

It is further assumed that the crack lies in an infinite medium, loaded by the stress field given by Atkinson and Eftaxiopoulos (1996) for the pure bond case or the stress field found in Sections 2.2.1 and 2.2.2 of this work for the pure slip case. Although this assumption discards the interaction between the crack on one hand and the open hole boundary, the steel/cement and the cement/rock interfaces on the other, it leads to a reasonable approximation to the actual problem. This approximation neglects the interaction of the crack elements with the hole and the steel/cement and the cement/rock interfaces. It corresponds to considering the dominant term in the integral equation for the crack, when this integral equation is turned into a Fredholm equation by inverting the singular part. An indication of how accurate this approximation

should be, can be seen by comparing results for a crack interacting with an elastic inclusion, by a complete calculation and by the approximation method (Atkinson, 1971). For the more complex variable path crack problem considered here, similar accuracy should be obtained.

3.1. In-plane problem

The stress and displacement field due to a dislocation in an infinite medium, at a point t in the complex plane $O(x_1,x_2)$, with complex Burger's vector b_1+ib_2 referred to the coordinate system $O(x_1,x_2)$ or Burger's vector $e^{i\alpha}(b'_1+ib'_2)$ referred to the coordinate system $O(x'_1,x'_2)$, which occurs after a rotation of $O(x_1,x_2)$ at an angle α (Fig. 1), is given (Tsamasphyros and Theocaris, 1982) by

$$\Phi(z)=\frac{\mu}{\pi i(\kappa+1)}\frac{C}{z-t} \tag{49}$$

$$\Psi(z)=\frac{\mu}{\pi i(\kappa+1)}\left[\frac{\overline{C}}{z-t}+\frac{C\bar{t}}{(z-t)^2}\right] \tag{50}$$

where

$$C=b_1+ib_2=e^{i\alpha}(b'_1+ib'_2) \tag{51}$$

μ is the shear modulus, $\kappa=3-4\nu$ for plain strain and ν is the Poisson's ratio. Stresses σ'_{11}, σ'_{22}, σ'_{12} and displacements u'_1, u'_2, with reference to the coordinate system $O(x'_1,x'_2)$, are given in terms of complex potentials $\Phi(z)$ and $\Psi(z)$ as

$$\sigma'_{11}+\sigma'_{22}=2\left[\Phi(z)+\overline{\Phi(z)}\right] \tag{52}$$

$$\sigma'_{22}-\sigma'_{11}+2i\sigma'_{12}=2e^{2i\alpha}[\bar{z}\Phi'(z)+\Psi(z)] \tag{53}$$

$$2\mu e^{i\alpha}(u'_1+iu'_2)=k\phi(z)-z\overline{\Phi(z)}-\overline{\psi(z)}+\text{constant} \tag{54}$$

From Eqs. (52) and (53) we immediately get

$$\sigma'_{22}+i\sigma'_{12}=\Phi(z)+\overline{\Phi(z)}+e^{2i\alpha}[\bar{z}\Phi'(z)+\Psi(z)] \tag{55}$$

The crack is now replaced by a distribution of dislocations of unknown density $\omega(t)$ in order to setup the relevant integral equation. We thus replace C in Eqs. (49) and (50) by

$$C=e^{i\alpha(t)}\omega(t)\,dt \tag{56}$$

where

$$\omega(t)=\frac{db'_1(t)+id b'_2(t)}{dt} \tag{57}$$

and $\alpha(t)$ is the angle of the inclination of the crack, at point t, with respect to the x_1-axis. From Eqs. (49), (50), (55) and (56) and by integrating over the crack line L we get

$$\int_L\frac{e^{i\alpha(t)}\omega(t)\,dt}{z-t}+\int_L\frac{e^{-i\alpha(t)}\overline{\omega(t)}\,d\bar{t}}{\bar{z}-\bar{t}}+e^{2i\alpha(z)}\int_L\frac{e^{-i\alpha(t)}\overline{\omega(t)}\,d\bar{t}}{z-t}-e^{2i\alpha(z)}\int_L\frac{e^{i\alpha(t)}(\bar{z}-\bar{t})\omega(t)\,dt}{(z-t)^2}$$
$$=-\frac{\pi i(\kappa^{(j)}+1)[[-p+\sigma'^{(j)}_{22}(z)]+i\sigma'^{(j)}_{12}(z)]}{\mu^{(j)}} \tag{58}$$

where $j = 1, 2, 3$ refer to the steel, the cement and the rock respectively, $\sigma_{22}^{\prime(j)}(z)$ and $\sigma_{12}^{\prime(j)}(z)$ are the normal and shear stresses applied along the crack line, in the absence of the crack, due to the remote earth's stresses and the pressure p acting on the borehole. Note that $p < 0$ when it is compressive on the crack edges. $\sigma_{22}^{\prime(j)}(z)$ and $\sigma_{12}^{\prime(j)}(z)$ are found by suitable transformations of the stresses that have been evaluated by Atkinson and Eftaxiopoulos (1996) for the perfect bond case, or are presented in Section 2.2.1 of this work for the perfect slip case.

The in-plane mode I and II CODs at any point z along the crack, can be evaluated from

$$b_1'(z) + \mathrm{i}b_2'(z) = \int_{t_B}^{z} \omega(t)\,\mathrm{d}t \tag{59}$$

if Eq. (57) is taken into account.

Let s, s_1 measure arc lengths along the crack line L starting from the point $|t_A| = R_1$. The total arc length of the curve L is l. We initially make the substitutions

$$\mathrm{d}z = \mathrm{e}^{\mathrm{i}\alpha^*(s_1)}\,\mathrm{d}s_1 \tag{60}$$

$$\mathrm{d}t = \mathrm{e}^{\mathrm{i}\alpha^*(s)}\,\mathrm{d}s \tag{61}$$

$$\alpha^*(s) = \alpha(t) \tag{62}$$

$$\alpha^*(s_1) = \alpha(z) \tag{63}$$

$$\omega(t) = \mathrm{e}^{-\mathrm{i}\alpha^*(s)}\omega^*(s) \tag{64}$$

$$\sigma_{22}^{\prime\,*(j)}(s_1) = \sigma_{22}^{\prime(j)}(z) \tag{65}$$

$$\sigma_{12}^{\prime\,*(j)}(s) = \sigma_{12}^{\prime(j)}(t) \tag{66}$$

into Eqs. (58) and (59), with

$$\omega^*(s) = \frac{\mathrm{d}b_1'^*(s) + \mathrm{i}\,\mathrm{d}b_2'^*(s)}{\mathrm{d}s} \tag{67}$$

$$b_k'^*(s) = b_k'(t) \quad \text{for } k = 1, 2 \tag{68}$$

Then, Eq. (58) becomes

$$\begin{aligned}
&\int_0^l \frac{\omega^*(s)\mathrm{e}^{\mathrm{i}\alpha^*(s)}\,\mathrm{d}s}{\int_0^{s_1}\mathrm{e}^{\mathrm{i}\alpha^*(s_1)}\,\mathrm{d}s_1 - \int_0^s \mathrm{e}^{\mathrm{i}\alpha^*(s)}\,\mathrm{d}s} + \int_0^l \frac{\overline{\omega^*(s)}\mathrm{e}^{-\mathrm{i}\alpha^*(s)}\,\mathrm{d}s}{\int_0^{s_1}\mathrm{e}^{-\mathrm{i}\alpha^*(s_1)}\,\mathrm{d}s_1 - \int_0^s \mathrm{e}^{-\mathrm{i}\alpha^*(s)}\,\mathrm{d}s} + \mathrm{e}^{2\mathrm{i}\alpha^*(s_1)} \\
&\quad\times \int_0^l \frac{\overline{\omega^*(s)}\mathrm{e}^{-\mathrm{i}\alpha^*(s)}\,\mathrm{d}s}{\int_0^{s_1}\mathrm{e}^{\mathrm{i}\alpha^*(s_1)}\,\mathrm{d}s_1 - \int_0^s \mathrm{e}^{\mathrm{i}\alpha^*(s)}\,\mathrm{d}s} - \mathrm{e}^{2\mathrm{i}\alpha^*(s_1)} \int_0^l \frac{\left[\int_0^{s_1}\mathrm{e}^{-\mathrm{i}\alpha^*(s_1)}\,\mathrm{d}s_1 - \int_0^s \mathrm{e}^{-\mathrm{i}\alpha^*(s)}\,\mathrm{d}s\right]}{\left[\int_0^{s_1}\mathrm{e}^{\mathrm{i}\alpha^*(s_1)}\,\mathrm{d}s_1 - \int_0^s \mathrm{e}^{\mathrm{i}\alpha^*(s)}\,\mathrm{d}s\right]^2}\mathrm{e}^{\mathrm{i}\alpha^*(s)}\omega^*(s)\,\mathrm{d}s \\
&\quad= -\frac{\pi\mathrm{i}(\kappa^{(j)}+1)[[-p + \sigma_{22}^{\prime\,*\,(j)}(s_1)] + \mathrm{i}\sigma_{12}^{\prime\,*\,(j)}(s_1)]}{\mu^{(j)}}
\end{aligned} \tag{69}$$

Further making the substitutions

$$s_1 = l y_1 \tag{70}$$

$$s = l y \tag{71}$$

$$\omega^{*}(s) = \frac{1}{l}\omega^{**}(y) \tag{72}$$

$$\alpha^{**}(y) = \alpha^{*}(s) \tag{73}$$

$$\alpha^{**}(y_1) = \alpha^{*}(s_1) \tag{74}$$

$$\sigma_{22}'^{**(j)}(y_1) = \sigma_{22}'^{*(j)}(s_1) \tag{75}$$

$$\sigma_{12}'^{**(j)}(y_1) = \sigma_{12}'^{*(j)}(s_1) \tag{76}$$

with

$$\omega^{**}(y) = \frac{\mathrm{d}b_1'^{**}(y) + \mathrm{i}\mathrm{d}b_2'^{**}(y)}{\mathrm{d}y} \tag{77}$$

$$b_k'^{**}(y) = b_k'(t) \quad \text{for } k = 1, 2 \tag{78}$$

into Eq. (69) we finally obtain

$$\int_0^1 K_1(y_1, y)\omega^{**}(y)\,\mathrm{d}y + \int_0^1 K_2(y_1, y)\overline{\omega^{**}(y)}\,\mathrm{d}y = -\sigma^{(j)}(y_1) \tag{79}$$

where

$$K_1(y_1, y) = \frac{1}{l}\left[\frac{1}{h(y_1) - h(y)} - \frac{\mathrm{e}^{2\mathrm{i}\alpha^{**}(y_1)}\left[\overline{h(y_1)} - \overline{h(y)}\right]}{\left[h(y_1) - h(y)\right]^2}\right]\mathrm{e}^{\mathrm{i}\alpha^{**}(y)} \tag{80}$$

$$K_2(y_1, y) = \frac{1}{l}\left[\frac{1}{\overline{h(y_1)} - \overline{h(y)}} + \frac{\mathrm{e}^{2\mathrm{i}\alpha^{**}(y_1)}}{h(y_1) - h(y)}\right]\mathrm{e}^{-\mathrm{i}\alpha^{**}(y)} \tag{81}$$

$$h(y) = \int_{-1}^{y} f(y)\,\mathrm{d}y \tag{82}$$

$$f(y) = \mathrm{e}^{\mathrm{i}\alpha^{**}(y)} \tag{83}$$

$$\sigma^{(j)}(y_1) = \frac{\pi\mathrm{i}(\kappa^{(j)} + 1)}{\mu^{(j)}}\left[\left[-p + \sigma_{22}'^{**(j)}(y_1)\right] + i\sigma_{12}'^{**(j)}(y_1)\right] \tag{84}$$

We then make the substitution

$$\omega^{**}(y) = \frac{\phi(y)\sqrt{y}}{\sqrt{1 - y}} \tag{85}$$

in Eq. (79) and get

$$\int_0^1 K_1(y_1, y)\frac{\phi(y)\sqrt{y}}{\sqrt{1 - y}}\,\mathrm{d}y + \int_0^1 K_2(y_1, y)\frac{\overline{\phi(y)}\sqrt{y}}{\sqrt{1 - y}}\,\mathrm{d}y = -\sigma^{(j)}(y_1) \tag{86}$$

The integral equations (86) are solved numerically by using the modified Lobatto–Chebyshev numerical quadrature rule (see e.g. Atkinson (1972) and Tsamasphyros and Theocaris (1982)). The mode I stress

intensity factor (SIF) is calculated from Eq. (A.5) (Appendix A). A numerical method that uses a binary search to locate an interval containing a zero of the function, then a combination of the methods of linear interpolation, extrapolation and bisection to locate the zero precisely, is implemented via the routine `c05agf` from the NAG library, for the determination of the pressure p that makes

$$K_{\mathrm{I}} = K_{\mathrm{IC}} \tag{87}$$

at each propagation step. K_{I} is the opening mode SIF and K_{IC} is the mode I fracture toughness.

As long as a straight crack is concerned, i.e. for the pure slip case and for rocks with low elasticity modulus in the pure bond case, the path of the fracture is known a priori. In the pure bond case, when there is a 90° rotation of the plane of the maximum tangential stress along the cement/rock interface, the propagating fracture will gradually turn, in order to become parallel to the plane of the maximum remote stress σ_{h} (see Fig. 1), eventually. In such a case the path of the crack is determined by using the maximum tangential stress criterion ahead of the crack tip.

3.2. Anti-plane shear mode crack analysis

The anti-plane analysis for the study of the crack under mode III COD, is analogous to the one presented above for the plane case. As in Atkinson and Eftaxiopoulos (1996), the stresses and displacements for the anti-plane problem can be written in terms of a complex potential $f(z)$ as

$$\sigma_{13} - \mathrm{i}\sigma_{23} = 2f'(z) \tag{88}$$

$$u_3 = \frac{1}{\mu^{(j)}}\left[f(z) + \overline{f(z)}\right] \tag{89}$$

For a single screw dislocation with Burger's vector b_3, at a point $z = t$ on the plane $\mathrm{O}(x_1, x_2)$, the complex potential $f(z)$ has the form

$$f(z) = -\frac{\mathrm{i}\mu^{(j)} b_3}{4\pi}\ln(z - t) \tag{90}$$

with $j = 1, 2, 3$ and the corresponding stresses and displacements are given by

$$\sigma'_{13} - \mathrm{i}\sigma'_{23} = -\frac{\mathrm{e}^{\mathrm{i}\alpha(z)}\mathrm{i}\mu^{(j)} b_3}{2\pi(z - t)} \tag{91}$$

$$u_3 = \frac{b_3 \tan^{-1}\frac{x_2}{x_1}}{2\pi} \tag{92}$$

if the fundamental solution given by Hirth and Lothe (1982) is taken into account. Replacing the crack by a continuous distribution of screw dislocations along the crack curve L, we get the integral equation

$$-\sigma^{(j)}(z) = \int_L \Im\left[\frac{\mathrm{e}^{\mathrm{i}\alpha(z)}\mathrm{i}}{z - t}\right] g(t)\,\mathrm{d}t \tag{93}$$

with

$$\sigma^{(j)}(z) = \frac{2\pi\sigma'^{j}_{23}(z)}{\mu^{(j)}} \tag{94}$$

$$g(t) = \frac{\mathrm{d}b_3(t)}{\mathrm{d}t} \tag{95}$$

Note that $\sigma_{23}^{ij}(z)$ is the anti-plane stress applied along the crack path L, in the absence of the crack. It can be deduced via suitable transformations from the stress field evaluated by Atkinson and Eftaxiopoulos (1996) for the perfect bond case or from Section 2.2.2 of this work for the perfect slip case. A similar numerical procedure to the one followed for the in-plane crack problem (Section 3.1) is adopted in the anti-plane case.

4. Analytical solution for a straight crack emanating from a cased and cemented wellbore

When the hydraulic fracture is straight, i.e. when $E^{(3)}$ is relatively big for the perfect bond case and always (See Section 5) for the perfect slip case, it is possible to solve the crack problem analytically. The crack propagates along the plane of the minimum remote earth's stress σ_h, i.e. along the x_1-axis and is open at the open hole. The analytical solution is much faster than the numerical one and it enables us to check the accuracy of our numerical results, as long as a straight crack is concerned. We again assume that the crack lies in an infinite medium, loaded by the appropriate stress field around the wellbore (see Sections 2.2.1 and 2.2.2).

4.1. In-plane problem

The crack, which extends from R_1 to a is now replaced by a distribution of dislocations in order to setup the relevant integral equation. Since the crack is along the x_1-axis, according to Eq. (51) we set

$$C = \mathrm{i}\omega(\xi)\,\mathrm{d}\xi \tag{96}$$

with

$$\omega(\xi) = \frac{\mathrm{d}b_2(\xi)}{\mathrm{d}\xi} \tag{97}$$

and from Eqs. (58), (96) and (97) we get

$$\int_{R_1}^{a} \frac{\omega(\xi)\,\mathrm{d}\xi}{x_1 - \xi} = \sigma^{(j)}(x_1) \tag{98}$$

where

$$\sigma^{(1)}(x_1) = \frac{\pi(\kappa^{(1)}+1)}{2\mu^{(1)}}(\sigma_{22}^{(1)}(x_1) - p) \quad \text{for } R_1 \leqslant \xi \leqslant R_2 \tag{99}$$

$$\sigma^{(2)}(x_1) = \frac{\pi(\kappa^{(2)}+1)}{2\mu^{(2)}}(\sigma_{22}^{(2)}(x_1) - p) \quad \text{for } R_2 \leqslant \xi \leqslant R_3 \tag{100}$$

$$\sigma^{(3)}(x_1) = \frac{\pi(\kappa^{(3)}+1)}{2\mu^{(3)}}(\sigma_{22}^{(3)}(x_1) - p) \quad \text{for } R_3 \leqslant \xi \tag{101}$$

where $\sigma_{22}^{(1)}(x_1)$, $\sigma_{22}^{(2)}(x_1)$ and $\sigma_{22}^{(3)}(x_1)$ are the normal stresses applied along the crack line, within the steel, the cement and the rock respectively, in the absence of the crack, due to the remote earth's stresses and due to the pressure p on the borehole. $\sigma_{22}^{(1)}(x_1)$, $\sigma_{22}^{(2)}(x_1)$ and $\sigma_{22}^{(3)}(x_1)$ have been found by Atkinson and Eftaxiopoulos (1996) for the pure bond case and are given from Eqs. (28) and (33) for the pure slip case.

Making the substitutions

$$\xi = \frac{a - R_1}{2}\xi' + \frac{a + R_1}{2} \tag{102}$$

$$x_1 = \frac{a - R_1}{2} x_1' + \frac{a + R_1}{2} \tag{103}$$

$$\omega'(\xi') = \omega(\xi) \tag{104}$$

$$\sigma'(x_1') = \sigma(x_1) \tag{105}$$

we eventually arrive at

$$\int_{-1}^{1} \frac{\omega'(\xi')\,\mathrm{d}\xi'}{x_1' - \xi'} = \sigma'^{(j)}(x_1') \tag{106}$$

Inverting Eq. (106), for the case of finite stress at the point $\xi = R_1$, i.e. when the crack is open at that point, we obtain

$$\omega'(\xi') = \frac{1}{\pi^2} \left\{ \frac{1 + \xi'}{1 - \xi'} \right\}^{1/2} \int_{-1}^{1} \left\{ \frac{1 - \xi'}{1 + \xi'} \right\}^{1/2} \frac{\sigma'^{(j)}(x_1')}{x_1' - \xi'}\,\mathrm{d}x_1' \tag{107}$$

Replacing $\omega'(\xi')$ by

$$\omega'(\xi') = \omega''(\xi') \left\{ \frac{1 + \xi'}{1 - \xi'} \right\}^{1/2} \tag{108}$$

we get

$$\begin{aligned} \omega''(\xi') = {} & \frac{1}{\pi^2} \int_{-1}^{b} \left\{ \frac{1 - \xi'}{1 + \xi'} \right\}^{1/2} \frac{\sigma'^{(1)}(x_1')}{x_1' - \xi'}\,\mathrm{d}x_1' + \frac{1}{\pi^2} \int_{b}^{c} \left\{ \frac{1 - \xi'}{1 + \xi'} \right\}^{1/2} \frac{\sigma'^{(2)}(x_1')}{x_1' - \xi'}\,\mathrm{d}x_1' \\ & + \frac{1}{\pi^2} \int_{c}^{1} \left\{ \frac{1 - \xi'}{1 + \xi'} \right\}^{1/2} \frac{\sigma'^{(2)}(x_1')}{x_1' - \xi'}\,\mathrm{d}x_1' \end{aligned} \tag{109}$$

where

$$b = \frac{2R_2}{a - R_1} - V \tag{110}$$

$$c = \frac{2R_3}{a - R_1} - V \tag{111}$$

$$V = \frac{a + R_1}{a - R_1} \tag{112}$$

since $\sigma'(x_1')$ is discontinuous along $r = R_2$, $r = R_3$. Making the substitutions

$$b = \cos\phi_1 \tag{113}$$

$$c = \cos\phi_2 \tag{114}$$

$$x_1' = \cos\phi \tag{115}$$

Eq. (109) becomes

$$\omega''(\xi') = \frac{1}{\pi^2}\int_{\phi_1}^{\pi}\frac{1-\cos\phi}{\cos\phi-\xi'}\sigma'^{(1)}(\cos\phi)\,\mathrm{d}\phi + \frac{1}{\pi^2}\int_{\phi_2}^{\phi_1}\frac{1-\cos\phi}{\cos\phi-\xi'}\sigma'^{(2)}(\cos\phi)\,\mathrm{d}\phi + \frac{1}{\pi^2}\int_{0}^{\phi_2}\frac{1-\cos\phi}{\cos\phi-\xi'}\sigma'^{(3)}(\cos\phi)\,\mathrm{d}\phi \tag{116}$$

Substituting $\sigma'^{(1)}(\cos\phi)$, $\sigma'^{(2)}(\cos\phi)$ and $\sigma'^{(3)}(\cos\phi)$ by their expressions from Atkinson and Eftaxiopoulos (1996) for the pure bond case or from Eqs. (28) and (33) for the perfect slip case, we eventually get

$$\begin{aligned}\omega''(\xi') = \frac{1}{2\pi}\Bigg\{ &\frac{\kappa^{(1)}+1}{\mu^{(1)}}\Big\{L_1^{(1)}[I_2(\xi')]_{\phi_1}^{\pi} + [M_1^{(1)}-p][T_0(\xi')]_{\phi_1}^{\pi} + N_1^{(1)}[I_{-2}(\xi')]_{\phi_1}^{\pi} + O_1^{(1)}[I_{-4}(\xi')]_{\phi_1}^{\pi}\Big\}\Bigg\}\\ &+\Bigg\{\frac{\kappa^{(2)}+1}{\mu^{(2)}}\Big\{L_1^{(2)}[I_2(\xi')]_{\phi_2}^{\phi_1} + [M_1^{(2)}-p][T_0(\xi')]_{\phi_2}^{\phi_1} + N_1^{(2)}[I_{-2}(\xi')]_{\phi_2}^{\phi_1} + O_1^{(2)}[I_{-4}(\xi')]_{\phi_2}^{\phi_1}\Big\}\\ &+\frac{\kappa^{(3)}+1}{\mu^{(3)}}\Big\{[M_1^{(3)}-p][T_0(\xi')]_{0}^{\phi_2} + N_1^{(3)}[I_{-2}(\xi')]_{0}^{\phi_2} + O_1^{(3)}[I_{-4}(\xi')]_{0}^{\phi_2}\Big\}\Bigg\}\end{aligned} \tag{117}$$

where

$$I_2(\xi') = \int\frac{(1-\cos\phi)(\cos\phi+V)^2}{\cos\phi-\xi'}\,\mathrm{d}\phi \tag{118}$$

$$T_0(\xi') = \int\frac{(1-\cos\phi)}{\cos\phi-\xi'}\,\mathrm{d}\phi \tag{119}$$

$$I_{-2}(\xi') = \int\frac{(1-\cos\phi)}{(\cos\phi-\xi')(\cos\phi+V)^2}\,\mathrm{d}\phi \tag{120}$$

$$I_{-4}(\xi') = \int\frac{(1-\cos\phi)}{(\cos\phi-\xi')(\cos\phi+V)^4}\,\mathrm{d}\phi \tag{121}$$

The indefinite integrals in Eqs. (118)–(121) have been evaluated by elementary analytical means.

For the pure bond case

$$L_1^{(j)} = 4\left(\frac{a-R_1}{2}\right)^2 C^{(j)} \tag{122}$$

$$N_1^{(j)} = F^{(j)}\left(\frac{a-R_1}{2}\right)^{-2} \tag{123}$$

$$O_1^{(j)} = G^{(j)}\left(\frac{a-R_1}{2}\right)^{-4} \tag{124}$$

$$M_1^{(j)} = 2A^{(j)} + D^{(j)} \tag{125}$$

for $j = 1, 2, 3$. Constants $A^{(j)}$, $C^{(j)}$, $D^{(j)}$, $F^{(j)}$, $G^{(j)}$ are given by Atkinson and Eftaxiopoulos (1996).

For the pure slip case

$$M_1^{(3)} = \sigma_h \tag{126}$$

$$N_1^{(3)} = -G^{(3)}\left(\frac{a-R_1}{2}\right)^{-2} \tag{127}$$

$$O_1^{(3)} = 6B^{(3)}\left(\frac{a-R_1}{2}\right)^{-4} \tag{128}$$

$$L_1^{(j)} = 6D^{(j)}\left(\frac{a-R_1}{2}\right)^{2} \tag{129}$$

$$M_1^{(j)} = 2C^{(j)} + \frac{F^{(j)}}{2} \tag{130}$$

$$N_1^{(j)} = -G^{(j)}\left(\frac{a-R_1}{2}\right)^{-2} \tag{131}$$

$$O_1^{(j)} = 6B^{(j)}\left(\frac{a-R_1}{2}\right)^{-4} \tag{132}$$

with $j = 1, 2$. Constants $B^{(j)}$, $C^{(j)}$, $D^{(j)}$, $G^{(j)}$ with $j = 1, 2, 3$ are found by solving a system of linear equations (see end of Section 2.2.1).

4.2. Analytical solution of the anti-plane problem

For a straight crack, Eq. (93) reduces to

$$\int_{R_1}^{a} \frac{g(\xi)\,\mathrm{d}\xi}{x_1 - \xi} = -\sigma(x_1) \tag{133}$$

with $\sigma(x_1)$ given from Eq. (94). That stress is given by Atkinson and Eftaxiopoulos (1996) for the pure bond case and from Section 2.2.2 for the pure slip case. The solution of Eq. (133) gives

$$g''(\xi') = \frac{2}{\pi}\left\{\frac{1}{\mu^{(1)}}\left\{M_2^{(1)}[T_0(\xi')]_{\phi_1}^{\pi} + N_2^{(1)}[I_{-2}(\xi')]_{\phi_1}^{\pi}\right\} + \frac{1}{\mu^{(2)}}\left\{M_2^{(2)}[T_0(\xi')]_{\phi_2}^{\phi_1} + N_2^{(2)}[I_{-2}(\xi')]_{\phi_2}^{\phi_1}\right\} + \frac{1}{\mu^{(3)}}\left\{M_2^{(3)}[T_0(\xi')]_{0}^{\phi_2} + N_2^{(3)}[I_{-2}(\xi')]_{0}^{\phi_2}\right\}\right\} \tag{134}$$

with

$$N_2^{(j)} = 2\Im[B^{(j)}]\left(\frac{a-R_1}{2}\right)^{-2} \tag{135}$$

$$M_2^{(j)} = 2\Im[A^{(j)}] \tag{136}$$

for $j = 1, 2, 3$. $A^{(j)}$, $B^{(j)}$ for the pure bond case are given by Atkinson and Eftaxiopoulos (1996).

For the pure slip case, we have the same solution form as Eq. (134). Due to the freely slipping interfaces, the only nonzero stresses are in the rock with the anti-plane stresses in the cement and the steel being zero. Hence $N_2^{(3)}$, $M_2^{(3)}$ are given from Eqs. (135) and (136) respectively, while $A^{(3)}$ and $B^{(3)}$ are defined by Eqs. (47) and (48).

5. Results

The Young's moduli and Poisson's ratios that we used for the steel and the cement were $E^{(1)} = 200$ GPa, $v^{(1)} = 0.27$ and $E^{(2)} = 10$ GPa, $v^{(2)} = 0.2$ respectively. The Young's modulus of the rock was either $E^{(3)} = 20$ or 2 GPa and Poisson's ratio of the rock was $v^{(3)} = 0.2$. The remotely applied earth in-plane stresses were $\sigma_H = -40$ MPa and $\sigma_h = -20$ MPa and the far field anti-plane stresses, developing due to a possible inclination of the borehole, were $\sigma_{13}^{\infty} = 10$ MPa and $\sigma_{23}^{\infty} = 5$ MPa (tensile stresses are taken to be positive). Radii $R_1 = 12.7$ cm, $R_2 = 14$ cm and $R_3 = 17.8$ cm were assigned to the open hole, the steel/cement and the cement/rock interfaces respectively. In all cases that we have studied we have assumed that the pressure is constant along the crack length. The crack was considered to be open at the casing. The initial crack length was taken as $1.00001(R_3 - R_1)$ and the length of the fracture at the final propagation step was $7R_3$. The normalized fracture toughness of the rock is taken as $\overline{K_{IC}} = (K_{IC}/(|\sigma_h|(R_3)^{1/2})) = 0.1$. During the propagation process, we required that the mode I opening displacement of the crack remains greater than 1 mm, all along it. If a smaller normal jump was encountered while $K_I \geqslant K_{IC}$, then a bigger pressure was sought in order to make the jump at that point equal to 1 mm. A variable number of collocation and integration points, increasing with the crack extension, was used at each propagation step.

5.1. Results for the stress field around a cased and cemented wellbore with purely bonded steel/cement and cement/rock interfaces

Results for this case have been presented by Atkinson and Eftaxiopoulos (1996). In that paper, it was observed that for low Young's moduli of the rock (e.g. 2, 3 and 4 GPa), the plane of the maximum tangential stress $\sigma_{\theta\theta}$ along the cement/rock interface, is rotated at 90° with respect to the plane of the maximum remote stress σ_h. Such an observation has been depicted in Fig. 2. The pressure in the well was taken

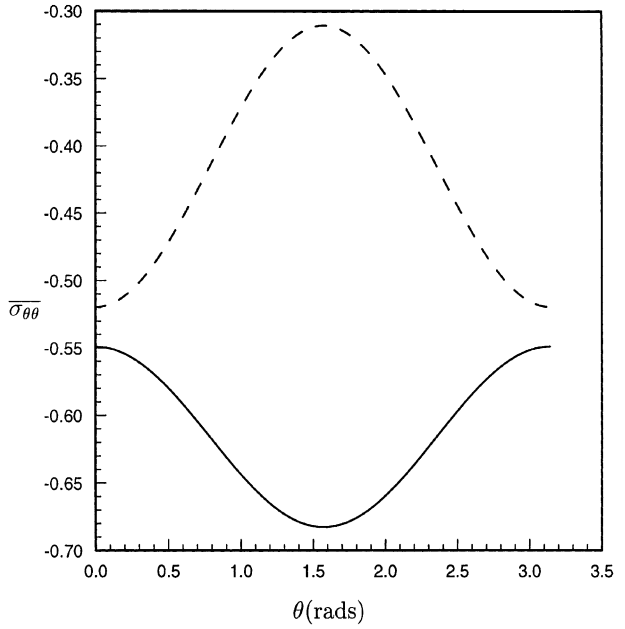

Fig. 2. Variation of the normalized tangential stress $\overline{\sigma_{\theta\theta}} = \sigma_{\theta\theta}/|p|$ versus the angle θ with $E^{(3)} = 2$ GPa for $r = R_2$ (—) and for $r = R_3$ (- - -).

$p = 35$ MPa. For larger values of Young's moduli of the rock, the plane of the maximum $\sigma_{\theta\theta}$ along the cement/rock interface, remained parallel to the plane of σ_h. Atkinson and Eftaxiopoulos (1996) developed a dimensionless quantity, depending on the Young's moduli E and the Poisson's ratios v of the rock, the steel and the cement and on the radii R_1, R_2 and R_3, that determines whether the plane of the maximum $\sigma_{\theta\theta}$ along the cement/rock interface, is at $\pi/2$ or at 0° with the x_1-axis (see Fig. 1). According to Atkinson and Eftaxiopoulos (1996), the two latter orientations are the only possible ones for the plane of the maximum $\sigma_{\theta\theta}$ along the cement/rock interface, for all Young's moduli of rocks. Hence, according to that analysis, we assume in this paper that an initial radial fracture pre-exists within the casing and the cement annuli, either at an angle of 90° or at 0° with the x_1-axis.

5.2. Results for the stress field around a cased and cemented wellbore with purely slipping steel/cement and cement/rock interfaces

The variation of the normalized tangential stress $\overline{\sigma_{\theta\theta}} = \sigma_{\theta\theta}/|p|$ with respect to θ, along the circular interfaces $r = R_1$, $r = R_2$ and $r = R_3$, is shown in Fig. 3, for two kinds of rock with $E^3 = 20$ and 2 GPa. Again the pressure in the well was taken $p = 35$ MPa. It is evident that the plane of the maximum tangential stress, along the fluid–steel, steel–cement and cement–rock interfaces, remains parallel to the plane of the maximum (in algebraic value) remotely applied normal stress σ_h, for both kinds of rock. This was also the case in several other examples that we tried, with bigger values for the elasticity modulus of the rock. Such a result is different from the corresponding result outlined in Section 5.1 for the perfect bond case, where the plane of the maximum $\sigma_{\theta\theta}$ along the cement/rock interface may rotate at 90° with respect to the remote stress σ_h. For the perfect bond case, Atkinson and Eftaxiopoulos (1996) used the 'equivalent inclusion' approach, where the open hole, the steel and the cement annuli were replaced by a single 'equivalent' inclusion. Thus a rule of thumb was developed, which related the elastic properties of the rock with the turning of the crack.

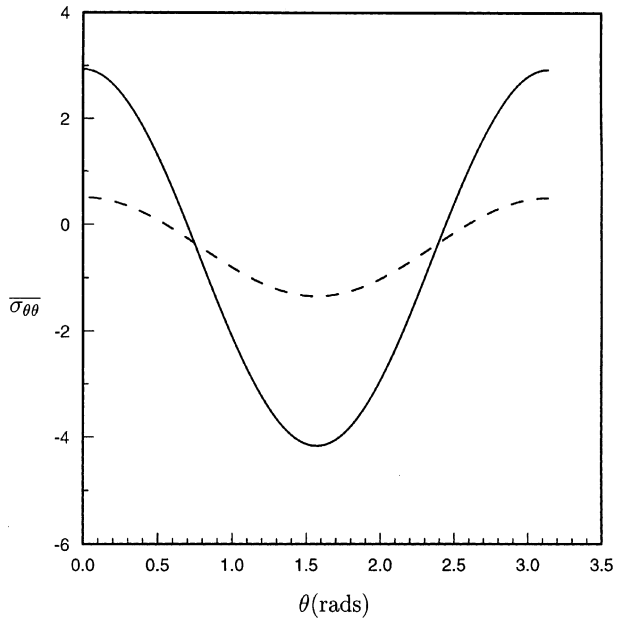

Fig. 3. Variation of the normalized tangential stress $\overline{\sigma_{\theta\theta}}$ versus the angle θ, with $E^{(3)} = 2$ GPa for $r = R_2$ (—), $r = R_3$ (- - -).

Such a simplified model was not possible for the perfect slip case, presumably because of the slipping that occurs between the steel, the cement and the rock.

5.3. Results for the hydraulic fracture propagation from a wellbore with purely bonded interfaces

In Fig. 4 the crack path corresponding to two different rock properties is illustrated. When $E^{(3)} = 2$ GPa the preferable angle for the initial crack, is $\pi/2$, due to the near wellbore effects caused by the presence of the steel and the cement (Atkinson and Eftaxiopoulos, 1996). Nevertheless, far from the hole the near wellbore effects decay and the fracture tends to orientate itself perpendicularly to σ_h. The turning process starts immediately after the crack enters the rock. On the other hand, when $E^{(3)} = 20$ GPa, the plane where the peak hoop stress $\sigma_{\theta\theta}$ acts, is not changed near the well and the crack propagates along a straight line.

The normalized pressure $\overline{p} = p/\sigma_h$ versus the normalized propagation length $\overline{l^{(k)}} = l^{(k)}/R_3$ is shown in Fig. 5. The pressures required for the propagation of the curved crack ($E^{(3)} = 2$ GPa, dashed line) are larger than the ones needed for the extension of the straight one ($E^{(3)} = 20$ GPa, solid line and dashed-dotted lines). The turning of the fracture, may make the requirement for a minimum mode I jump $b_2'(z) = 1$ mm more difficult to achieve, than in the straight crack case (see Fig. 6). Thus the pressure is increased. Pressures in both cases tend to values close to σ_h for long cracks, since $\overline{K_{IC}} = 0.1$ i.e. close to zero. The agreement between the numerical results (solid line) and the analytical results (dashed-dotted line) for a straight crack ($E^{(3)} = 20$ GPa) is good. The kink in the beginning of the solid and the dashed-dotted lines, is due to the requirement for a minimum mode I jump $b_2'(z) = 1$ mm at the first propagation step.

Fig. 6 depicts the variation of the normalized mode I opening displacement $\overline{b_2'(z)}$ of the crack with respect to the normalized arc length $\overline{s_n}$ (see Eq. (71)) along it, for the two cracks shown in Fig. 4, at the last propagation step. The most significant changes take place close to the wellbore presumably as a result of the presence of the cement and the casing. Close to the open hole ($\overline{s_n} = 0$) the opening of the crack is reduced, presumably due to the presence of the steel casing. Note that a negative jump $b_2'(z)$ was encountered close to $\overline{s_n} = 0$ while $K_I \geqslant K_{IC}$, in the curved crack case. Subsequently a bigger pressure, which made $b_2'(z) = 1$ mm at that point, was found. A significant reduction in the COD occurs in the curved crack case (dashed line) between $\overline{s_n} = 0.5$ and 1. This is possibly due to the severe turning of the crack that occurs (see Fig. 4) at such distances from the wellbore.

The fluctuation of the normalized shear opening displacement $\overline{b_1'(z)}$ of the crack versus the normalized arc length $\overline{s_n}$, is presented in Fig. 7 for the cracks of Fig. 4. The most severe mode II crack deformation develops close to the wellbore where the most significant turning of the crack takes place.

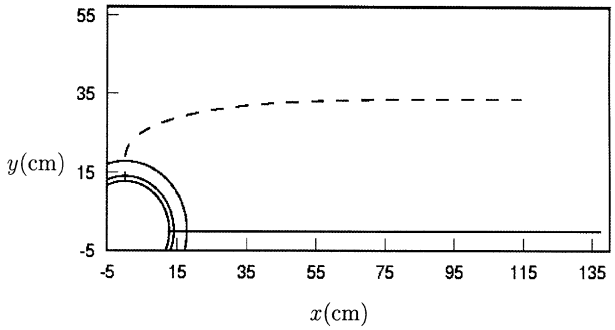

Fig. 4. Fracture propagation from a cased, cemented and inclined wellbore into two different rocks, having elasticity moduli $E^{(3)} = 20$ GPa (—) and $E^{(3)} = 2$ GPa (- - -) respectively.

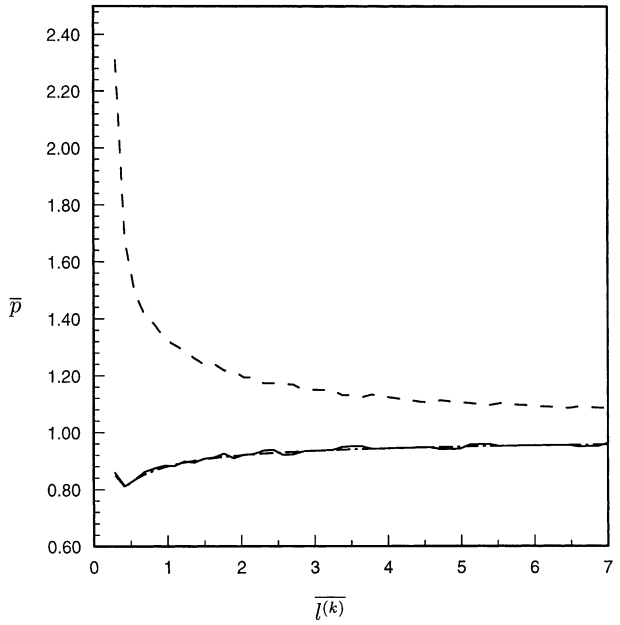

Fig. 5. The normalized pressure $\overline{p} = p/\sigma_{\mathrm{h}}$ versus the normalized crack length $\overline{l^{(k)}} = l^{(k)}/R_3$ for two different rocks with $E^{(3)} = 20$ GPa (solid line for the numerical result and dashed-dotted line for the analytical result) and $E^{(3)} = 2$ GPa (dashed line for the numerical result).

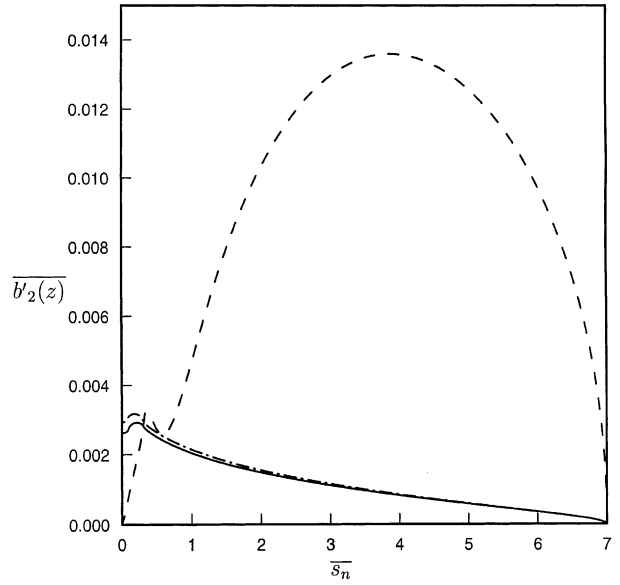

Fig. 6. The normalized mode I COD $\overline{b'_2(z)} = b'_2(z)/R_3$ versus the normalized arc length $\overline{s_n} = s_n/R_3$, at the final propagation step, for two different rocks with $E^{(3)} = 20$ GPa (solid line for the numerical result and dashed-dotted line for the analytical result) and $E^{(3)} = 2$ GPa (dashed line for the numerical result).

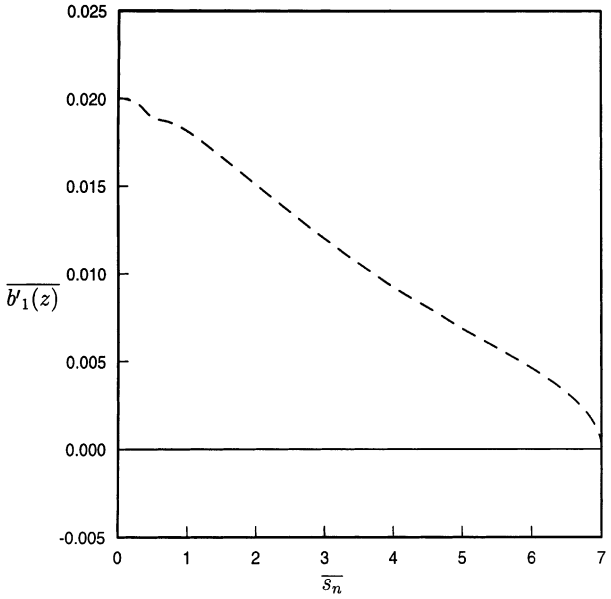

Fig. 7. The normalized mode II COD $\overline{b'_1(z)} = b'_1(z)/R_3$ of the crack versus the normalized arc length $\overline{s_n} = s_n/R_3$, at the final propagation step, for two different rocks with $E^{(3)} = 20$ GPa (—) and $E^{(3)} = 2$ GPa (dashed line for the numerical result).

Finally, in Fig. 8 the dependence of the normalized mode III COD $\overline{b_3(z)}$ on the normalized arc length $\overline{s_n}$, at the final propagation step, is monitored. The effect of the casing and the cement is mostly sensed when we have a small—relatively to the steel and the cement—elasticity modulus $E^{(3)} = 2$ GPa for the rock. Since the amount of mode III COD, should give a qualitative measure of the tendency of a 3D crack surface to twist, Fig. 8 indicates that (especially for $E^{(3)} = 2$ GPa) the twisting process would start further from the wellbore.

5.4. Results for the hydraulic fracture propagation from a wellbore with purely slipping interfaces

When slipping interfaces are considered, there is no turning of the plane of the maximum tangential stress, along the cement/rock interface, if the Young's modulus of the rock is changed (see Fig. 3). Hence the hydraulic fracture is always straight. In Fig. 9 the pressure variation with respect to the propagation length is shown, for two different rocks with $E^{(3)} = 20$ and 2 GPa. A comparison of the pressure profile for a straight crack (i.e. for $E^{(3)} = 20$ GPa), for the pure slip (Fig. 9) and the pure bond (Fig. 5) cases, shows that during the first propagation step, a bigger pressure is required for the pure slip case.

In Figs. 10 and 11 the variation of the normalized opening mode and anti-plane shear mode jumps, along the crack at the final propagation step, are depicted. Close to the open hole there is a reduction in the magnitude of the mode I COD, due to the presence of the steel casing which is much stiffer than the cement and the rock. Comparing results for the mode I COD, between the pure bond case (Fig. 6) and the pure slip case (Fig. 10), for $E^{(3)} = 20$ GPa, we notice that the crack opening is almost the same along the crack, for both cases. The anti-plane shear mode opening, vanishes inside the cement and the steel annuli because of the purely slipping cement/rock and steel/cement interfaces (see Section 4.2). Anti-plane CODs are roughly the same for the pure bond and the pure slip cases (Figs. 8 and 11), for a straight crack, i.e. for $E^{(3)} = 20$ GPa.

Since the crack is always straight in the pure slip case, lying along the plane of the maximum remote stress σ_h, no in-plane shear mode crack opening develops.

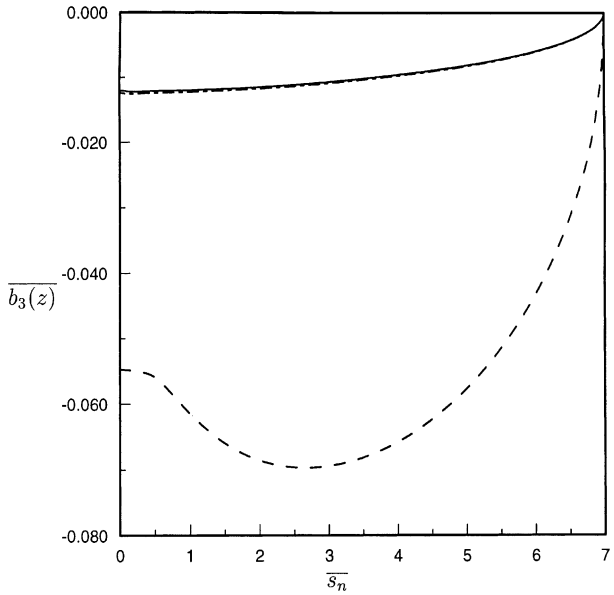

Fig. 8. The normalized mode III COD $\overline{b_3(z)} = b_3(z)/R_3$ versus the normalized arc length $\overline{s_n} = s_n/R_3$ during the last propagation step, for two different rocks with $E^{(3)} = 20$ GPa (solid line for the numerical result and dashed-dotted line for the analytical result) and $E^{(3)} = 2$ GPa (dashed line for the numerical result).

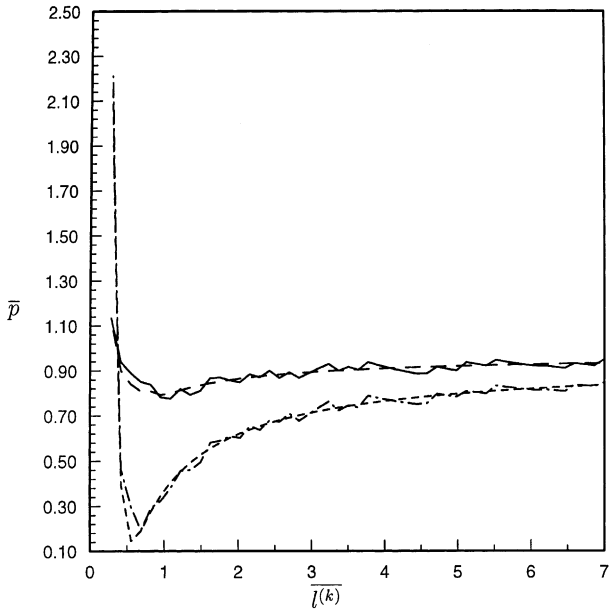

Fig. 9. The normalized pressure $\overline{p} = p/\sigma_h$ versus the normalized crack length $\overline{l^{(k)}} = l^{(k)}/R_3$ for two different rocks, with $E^{(3)} = 20$ GPa (solid line for the numerical result and dashed line (long dashes) for the analytical result) and $E^{(3)} = 2$ GPa (dashed-dotted line for the numerical result and dashed line (short dashes) analytical result).

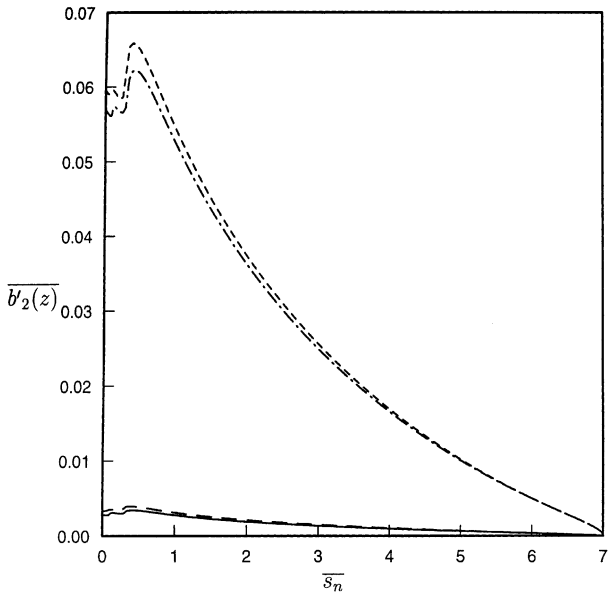

Fig. 10. The normalized mode I COD $\overline{b'_2(z)} = b'_2(z)/R_3$ versus the normalized arc length $\overline{s_n} = s_n/R_3$, at the final propagation step, for two different rocks with $E^{(3)} = 20$ GPa (solid line for the numerical result and dashed line (long dashes) for the analytical result) and $E^{(3)} = 2$ GPa (dashed-dotted line for the numerical result and dashed line (short dashes) for the analytical result).

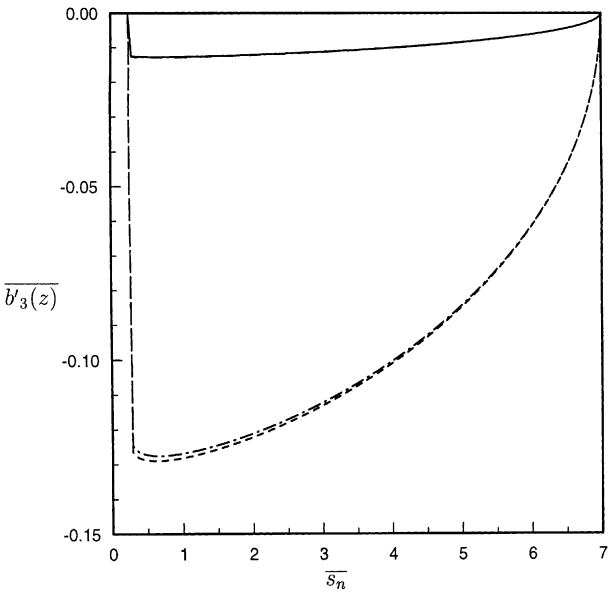

Fig. 11. The normalized mode III COD $\overline{b'_3(z)} = b'_3(z)/R_3$ versus the normalized arc length $\overline{s_n} = s_n/R_3$, at the final propagation step, for two different rocks with $E^{(3)} = 20$ GPa (solid line for the numerical result and dashed line (long dashes) for the analytical result) and $E^{(3)} = 2$ GPa (dashed-dotted line for the numerical result and dashed line (short dashes) for the analytical result).

5.5. Results for a starter crack with varying orientation or with varying elastic modulus of the rock

A straight starter crack, i.e. a crack at the first propagation step, whose length is $1.00001(R_3 - R_1)$, is considered in this subsection. The crack is either parallel to the x_1-axis and the elastic modulus of the rock varies from 2 to 50 GPa or the orientation of the crack varies from 0 to $\pi/2$ with respect to the x_1-axis while the elastic modulus of the rock remains constant and equal to 20 GPa.

In Figs. 12–14 the variations of the pressure, the mode I COD at $r = R_1$ and the mode III COD at $r = R_1$ with respect to varying elastic modulus of the rock $E^{(3)}$, for a starter crack parallel to the x_1-axis are shown. The pressure needed to propagate the crack further is greater in the pure slip case than in the pure bond case. In both cases the pressure decreases with increasing $E^{(3)}$ (Fig. 12). Analogous remarks can be made for the mode I COD (Fig. 13). Note that in the pure bond case, the crack tends to close for $E^{(3)} > 8.5$ GPa, but a bigger pressure is sought such that we have the minimum mode I opening $b_2 = 1$ mm at $r = R_1$. Regarding the mode III COD (Fig. 14), it increases with increasing $E^{(3)}$, as long as the pure bond case is concerned. In the pure slip case $b_3 = 0$ mm.

In Figs. 15–18 the variations of the pressure, the mode I COD at $r = R_1$, the mode II COD at $r = R_1$ and the mode III COD at $r = R_1$ with respect to varying angle θ between the straight starter crack and the x_1-axis, are shown. The pressure is greater for the pure slip case than for the pure bond one, for approximately $\theta < 45°$, while the opposite happens for $\theta > 45°$ (Fig. 15). Monotonically increasing pressure develops in the pure bond case while in the pure slip case does not. The kink in the graph for the pure slip case is due to the need for a sudden increase in pressure in order to avoid a negative mode I COD, i.e. in order to ensure that the minimum $b_2' = 1$ mm.

Fig. 16 indicates that the mode I COD decreases as the starter crack rotates, approaching the plane of the minimum remote stress σ_H. Values for the pure slip case are generally bigger than those for the pure

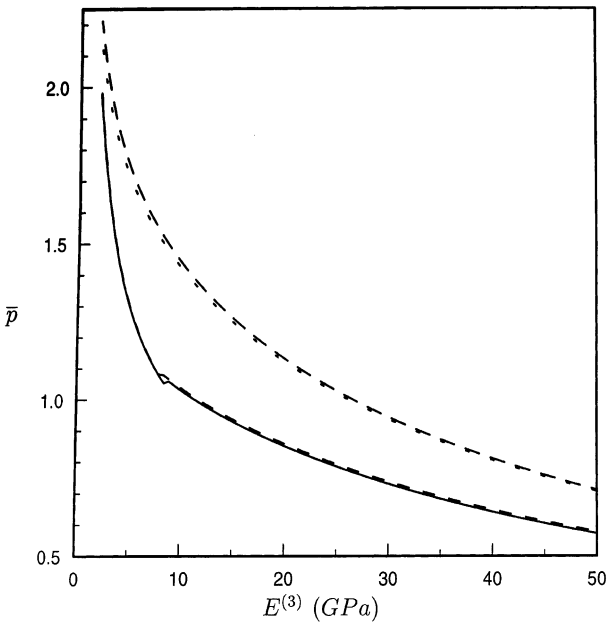

Fig. 12. The normalized pressure $\overline{p} = p/\sigma_h$ versus the elastic modulus $E^{(3)}$ of the rock for a starter crack parallel to the x_1-axis (solid line for the analytical result—pure bond case, dashed line (short dashes) for the numerical result—pure bond case, dashed line (very short dashes) for the analytical result—pure slip case, dashed line (long dashes) for the numerical result—pure slip case).

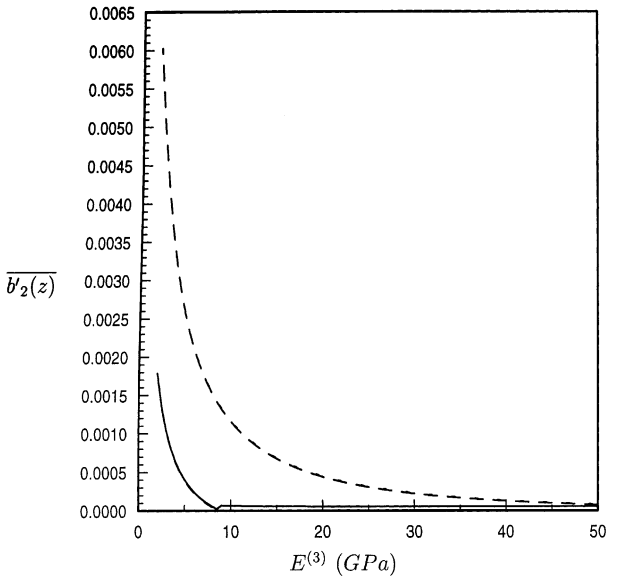

Fig. 13. The normalized mode I COD $\overline{b'_2(z)} = b'_2(z)/R_3$ versus the elastic modulus $E^{(3)}$ of the rock for a starter crack parallel to the x_1-axis (solid line for the analytical result—pure bond case, dashed line (short dashes) for the numerical result—pure bond case, dashed line (very short dashes) for the analytical result—pure slip case, dashed line (long dashes) for the numerical result—pure slip case).

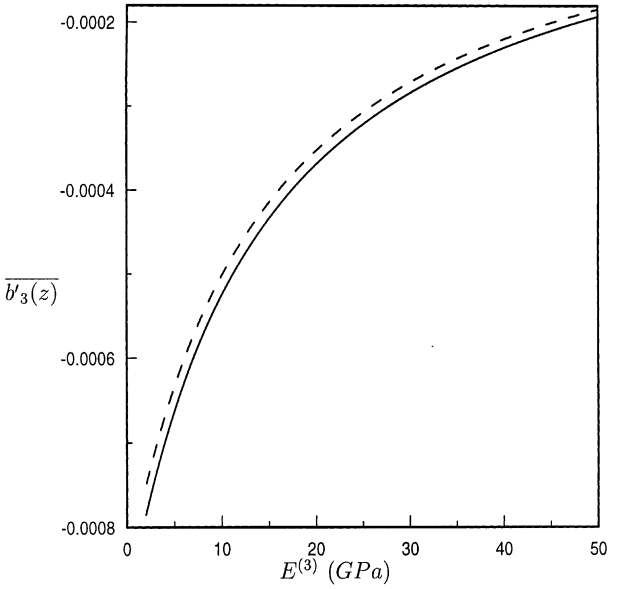

Fig. 14. The normalized mode III COD $\overline{b'_3(z)} = b'_3(z)/R_3$ versus the elastic modulus $E^{(3)}$ of the rock for a starter crack parallel to the x_1-axis (solid line for the analytical result—pure bond case, dashed line (short dashes) for the numerical result—pure bond case).

bond case. Due to negative CODs that were encountered for low angles θ, the required opening of $b'_2 =$ 1 mm is reached at low angles θ for the pure bond case.

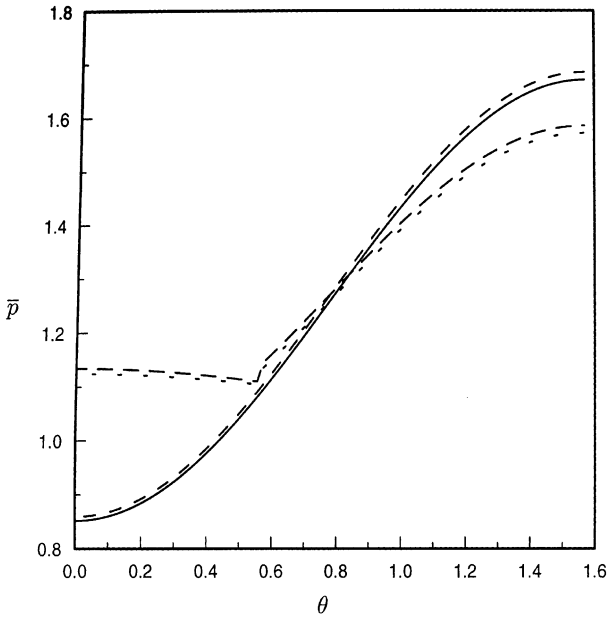

Fig. 15. The normalized pressure $\overline{p} = p/\sigma_h$ versus the angle θ between the straight starter crack and the x_1-axis, with $E^{(3)} = 20$ GPa (solid line for the analytical result—pure bond case, dashed line (short dashes) for the numerical result—pure bond case, dashed line (very short dashes) for the analytical result—pure slip case, dashed line (long dashes) for the numerical result—pure slip case).

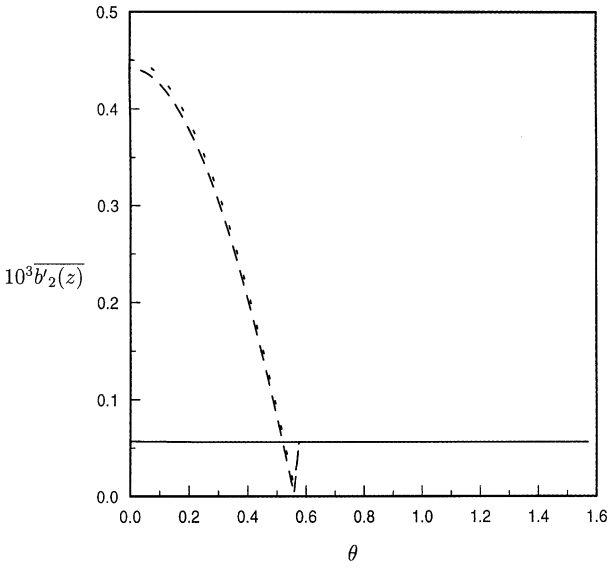

Fig. 16. The normalized mode I COD $\overline{b'_2(z)} = b'_2(z)/R_3$ at $r = R_1$, versus the angle θ between the straight starter crack and the x_1-axis, with $E^{(3)} = 20$ GPa (solid line for the analytical result—pure bond case, dashed line (short dashes) for the numerical result—pure bond case, dashed line (very short dashes) for the analytical result—pure slip case, dashed line (long dashes) for the numerical result—pure slip case).

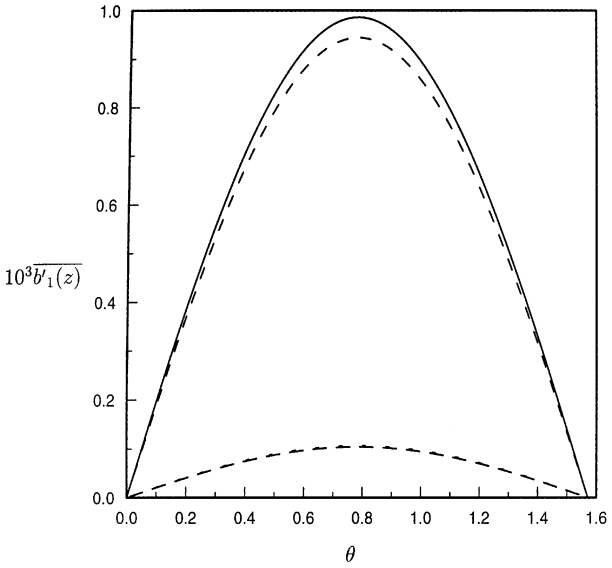

Fig. 17. The normalized mode II COD $\overline{b'_1(z)} = b'_1(z)/R_3$ at $r = R_1$ versus the angle θ between the straight starter crack and the x_1-axis, with $E^{(3)} = 20$ GPa (solid line for the analytical result—pure bond case, dashed line (short dashes) for the numerical result—pure bond case, dashed line (very short dashes) for the analytical result—pure slip case, dashed line (long dashes) for the numerical result—pure slip case).

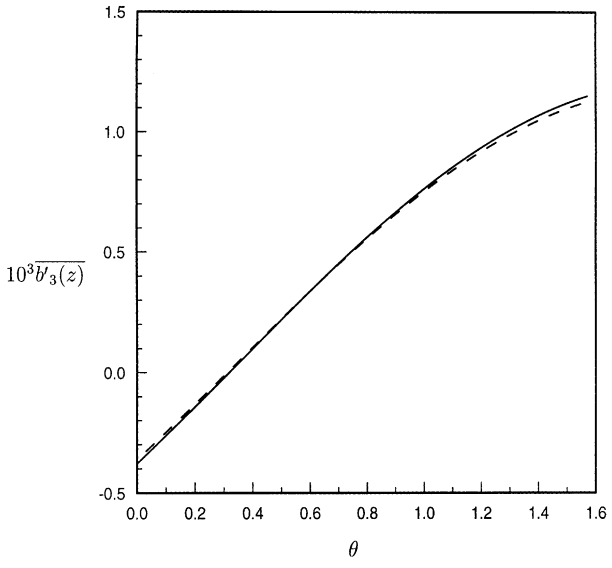

Fig. 18. The normalized mode III COD $\overline{b'_3(z)} = b'_1(z)/R_3$ at $r = R_1$ versus the angle θ between the straight starter crack and the x_1-axis, with $E^{(3)} = 20$ GPa (solid line for the analytical result—pure bond case, dashed line for the numerical result—pure bond case).

Fig. 17 indicates that the mode II COD at $r = R_1$ is bigger in the pure bond case than in the pure slip case, for all angles θ.

Changing signs characterize the variation of the mode III COD with θ (Fig. 18). If one assumes that the magnitude of b_3' is a measure of the tendency of the crack to twist, then opposite twisting angles may be expected for different angles θ of the starter crack with the x_1-axis.

6. Conclusions

A plane 2D model for the problem of hydraulic fracturing from a cased and cemented wellbore has been developed in this paper. Anti-plane calculations have also been pursued in an attempt to capture the qualitative features of the twisting of a real 3D crack surface. Two extreme boundary condition cases have been considered; pure bond and pure slip between the steel/cement and the cement/rock interfaces. Constant pressure is assumed along the hydraulic fracture. Analytical results for the tangential stress $\sigma_{\theta\theta}$ along the steel/cement and the cement/rock interfaces have been obtained. Numerical and analytical results for the pressure profile in the crack and for the mode I, II and III CODs have been presented.

The main results indicate that

- A rotation of 90° of the plane of the maximum tangential stress $\sigma_{\theta\theta}$ happens between the steel/cement and the cement/rock interfaces, in the pure bond boundary condition case, for rocks with low Young's modulus (e.g. 2, 3 and 4 GPa). The same conclusion was also reached by Atkinson and Eftaxiopoulos (1996). In the pure slip case no such rotation is observed and the plane of the maximum tangential stress $\sigma_{\theta\theta}$ remains parallel to the plane of the maximum remote stress σ_h, along both the steel/cement and the cement–rock interfaces, independent from the Young's modulus of the rock. Since we place the pre-existing initial radial crack along the plane of the maximum $\sigma_{\theta\theta}$ on the cement/rock interface, the hydraulic fracture may turn while propagating away from the wellbore in the pure bond case. In the pure slip case the fracture remains straight for any value of the Young's modulus of the rock.
- During the first propagation step, a bigger pressure is needed for the crack extension in the pure slip case than in the pure bond case, as long as a straight crack is concerned. Hence the not perfectly bonded steel and cement annuli, may not necessarily facilitate the first propagation step.
- The mode I COD at the wellbore, of a long straight crack, is roughly the same for both the pure bond and the pure slip cases. However in the pure slip case, such an opening increases as the Young's modulus of the rock decreases. Along the turning part of a curved crack the mode I COD is reduced, thus hindering fluid flow.
- Along a long straight fracture the mode III COD remains roughly unaltered for both the pure bond and the pure slip cases. Since we expect that the value of the mode III COD should give a qualitative measure of the tendency of a 3D crack surface to twist, the twisting process may not be affected by the boundary conditions at the wellbore. On the contrary the twisting process may be more severe for more compiant rocks.
- For a starter crack, parallel to the plane of the maximum remote stress σ_h, the pressure and the mode I COD at the hole ($r = R_1$) decrease as the elastic modulus of the rock increases. Bigger values for both the pressure and the mode I COD at the hole ($r = R_1$), develop in the pure slip case than in the pure bond case. On the contrary, the mode III COD at $r = R_1$ increases with increasing $E^{(3)}$, possibly indicating a more severe tendency for twist of the fracture in stiffer rocks.
- For a starter crack, inclined at an angle θ with respect to the x_1-axis and for a rock with $E^{(3)} = 20$ GPa, the pressure is greater in the pure slip case than in the pure bond case for $\theta < 45°$. The opposite happens for $\theta > 45°$. The mode I COD at the hole ($r = R_1$) decreases as the starter crack rotates. Values for the pure slip case are generally bigger than those for the pure bond case. The mode II COD at $r = R_1$ is bigger in the pure bond case than in the pure slip case, for all angles θ. Changing signs in the mode III COD evolution may indicate opposite angles of twist for a real 3D crack.

7. Discussion—limitations

The 2D model presented in this paper, for the propagation of a hydraulic fracture from a cased and cemented wellbore, cannot obviously capture all the features of the physical 3D phenomenon. Our model should be adequate, when the borehole axis is parallel to one of the far field principal axes, i.e. when the 3D fracture surface does not twist and remains parallel to the borehole axis. In that case our 2D plane strain approach should be sufficient and the anti-plane analysis is not needed. However, when the borehole axis is not parallel to one of the far field principal axes, we cannot address properly the turning and twisting processes of the 3D fracture surface, as it progressively reorients itself parallel to the plane of the far field maximum stress. In fact, the creation of multiple smaller fractures starting from a 3D crack surface during the twisting process, complicates even a 3D analysis. In this work, we calculate the mode III COD of the plane crack, which may give us a qualitative measure of the tendency of a real 3D crack to twist.

Our model does not also deal with perforations, which are used for the communication of the cased wellbore with the pay zone (i.e. the rock that contains the oil). The perforations are also used to trigger the initiation of the fracture. There are cases when a small starter fracture initiates from each perforation and all these flaws join up to form a single bigger crack further from the wellbore. Also, the perforations may be placed at regular angular intervals around the wellbore, since the location of the crack initiation is not known a priori. In our model we incorporate a single radial preexisting starter crack, as long as the width of the steel and cement annuli. We place this starter crack parallel to the plane of the maximum $\sigma_{\theta\theta}$ that develops on the cement/rock interface and thus we have the opportunity to study both curved and straight fracture propagations.

Appendix A. Evaluation of the in-plane mode I stress intensity factor and of the CODs

For the numerical procedure we have evaluated the SIF from displacement relations and for the analytical procedure from stress relations.

A.1. Numerical solution

From Eq. (57), the jump in the displacement at a point z along the crack can be written as

$$b_1'(z) + \mathrm{i}b_2'(z) = \int_{t_B}^{z} \omega(t)\,\mathrm{d}t \tag{A.1}$$

Alternatively we can write

$$b_1'^{**}(y_1) + \mathrm{i}b_2'^{**}(y_1) = \int_1^{y_1} \frac{\phi(y)\sqrt{y}}{\sqrt{1-y}}\,\mathrm{d}y \tag{A.2}$$

Taking the limit $y_1 \to 1^-$, we get

$$b_1'^{**}(1-\epsilon) - \mathrm{i}b_2'^{**}(1-\epsilon) = -\overline{\phi(1)}\sqrt{2\epsilon} \tag{A.3}$$

where $\epsilon \to 0$. From Kanninen and Popelar (1985), Eqs. (84) and (86) it can also be deduced that

$$b_1'^{**}(1-\epsilon) - \mathrm{i}b_2'^{**}(1-\epsilon) = -\frac{\mathrm{i}(\kappa^{(j)}+1)\sqrt{l}}{2\mu\sqrt{\pi}}[K_{\mathrm{I}}' + \mathrm{i}K_{\mathrm{II}}']\sqrt{\epsilon} \tag{A.4}$$

From Eqs. (A.3) and (A.4) we find

$$K_{\mathrm{I}}' + \mathrm{i}K_{\mathrm{II}}' = -\frac{2\sqrt{2}\mathrm{i}\sqrt{\pi}\mu^{(j)}}{\sqrt{l}(\kappa^{(j)}+1)}\overline{\phi(1)} \tag{A.5}$$

The in-plane CODs can be obtained from Eq. (A.2) by applying the numerical quadrature scheme that was used for the solution of Eq. (86). The mode III jump of the crack can be deduced from Eq. (A.2) if $\phi(y)$ is replaced by $\psi(y)$.

A.2. Analytical solution

From Eq. (97), the displacement jump across the crack flanks, at any point x_1 along the crack, can be evaluated from the relation

$$\int_a^{x_1} \omega(x)\,\mathrm{d}x = b_2(x_1) \tag{A.6}$$

or via the relation

$$\frac{(a-R_1)}{2}\int_{\phi_2}^{0} \omega''(\cos\psi)(1+\cos\psi)\,\mathrm{d}\psi = b_2(x_1) \tag{A.7}$$

where

$$\cos\phi_2 = x_1' \tag{A.8}$$

$$x_1 = \frac{a-R_1}{2}x_1' + \frac{a+R_1}{2} \tag{A.9}$$

$$\cos\psi = \xi' \tag{A.10}$$

$$\xi = \frac{a-R_1}{2}\xi' + \frac{a+R_1}{2} \tag{A.11}$$

The integral in Eq. (A.7) was evaluated by using the trapezium rule since the discrete values of the density are known from Eqs. (134) and (117).

From Eqs. (98), (101)–(105) we can express the stress, generated by the distribution of dislocations that we have already calculated from Eq. (117) near the crack tip, outside the crack as

$$\sigma''^{(3)}(1+\epsilon) = -\frac{4\mu^{(3)}}{\kappa^{(3)}+1}\frac{\omega''^{(1)}}{\sqrt{2\epsilon}} \tag{A.12}$$

where

$$\sigma''(x_1') = \sigma(x_1) \tag{A.13}$$

From the definition of the opening mode stress intensity factor K_{I}

$$K_{\mathrm{I}} = \lim_{x_1\to a}\sqrt{2\pi(x_1-a)}\sigma_{22}^{(3)}(x_1) \tag{A.14}$$

and from Eqs. (A.12) and (A.14), we finally obtain

$$K_{\mathrm{I}} = -2\sqrt{2\pi(a-R_2)}\frac{\mu^{(3)}}{\kappa^{(3)}+1}g(1) \tag{A.15}$$

References

Atkinson, C., 1971. A simple approximation for calculating the effect of inclusions on fracture. Scripta Metallurgica 5, 643–650.

Atkinson, C., 1972. On dislocation densities and stress singularities associated with cracks and pile-ups in inhomogeneous media. International Journal of Engineering Science 10, 45–71.

Atkinson, C., Eftaxiopoulos, D.A., 1996. A plane model for the stress field around an inclined cased and cemented wellbore. International Journal for Numerical and Analytical Methods in Geomechanics 20, 549–569.

Atkinson, C., Thiercelin, M., 1993. The interaction between the wellbore and pressure induced fractures. International Journal of Fracture 59, 23–40.

Carter, B.J., Wawrzynek, P.A., Ingraffea, A.R., 1994. Effects of casing and interface behavior in hydraulic fracture. In: Siriwardane, H.J., Zaman, M.M. (Eds.), Proceedings of the 8th International Conference on Computer Methods and Advances in Ceomechanics, Morgantown, West Virginia, USA, 22–28 May 1994. A.A. Balkema Publishers, Rotterdam, pp. 1561–1566.

Coker, E.G., Filon, L.N.G., 1957. A Treatise on Photo-Elasticity. Cambridge University Press, Cambridge (revised by Jessop, H.T.).

Eftaxiopoulos, D.A., Atkinson, C., 1996. Hydraulic fracture propagation from a cased, cemented and inclined wellbore. In: Aubertin, M., Hassani, F., Mitri, H. (Eds.), Proceedings of the 2nd North American rock Mechanics Symposium, Montreal, Canada, 19–21 June 1996. A.A. Balkema Publishers, Rotterdam, pp. 1127–1134.

Hirth, J.P., Lothe, J., 1982. Theory of Dislocations. Wiley, New York.

Kanninen, M.F., Popelar, C.H., 1985. Advanced Fracture Mechanics. Oxford University Press, Oxford.

Morales, R.H., Brady, B.H., 1993. Three dimensional analysis and visualization of the wellbore and the fracturing process in inclined wells. SPE Rocky Mountain Regional/Low Permeability Reservoirs Symposium, Denver, USA, 12–14 April, SPE 25889.

Romero, J., Mack, M.G., Elbel, J.L., 1995. Theoretical model and numerical investigation of near wellbore effects in hydraulic fracturing. SPE Annual Conference and Exhibition, Dallas, USA, 22–25 October, SPE 30506.

Tsamasphyros, G., Theocaris, P.S., 1982. Integral equation solution for half planes bonded together or in contact and containing internal cracks or holes. Ingenieur Archiv 53, 225–241.

Weng, X., 1993. Fracture initiation and propagation from deviated wellbores. 68th Annual Technical Conference and Exhibition, Houston, USA, 3–6 October, SPE 26597.

Yew, C.H., Li, Y., 1987. Fracturing of a deviated well. 62th Annual Technical Conference and Exhibition, Dallas, USA, 27–30 September, SPE 16930.

Yew, C.H., Schmidt, J.H., Li, Y., 1989. On fracture design of deviated wells. 64th Annual Technical Conference and Exhibition, San Antonio, USA, 8–11 October, SPE 19722.

Yew, C.H., Mear, M.E., Chang, C.C., Zhang, X.C., 1993. On perforating and fracturing of deviated cased wellbores. 68th Annual Technical Conference and Exhibition, Houston, USA, 3–6 October, SPE 26514.